Accelerated Estimation of Sea Spray-Mediated Heat Flux Using Gaussian Quadrature: Case Studies with a Coupled CFSv2.0-WW3 System

Ruizi Shi[1] and Fanghua Xu[1*]

[1] Department of Earth System Science, Ministry of Education Key Laboratory for Earth System Modeling, Institute for Global Change Studies, Tsinghua University, Beijing, 100084, China.

Correspondence to: Fanghua Xu (fxu@mail.tsinghua.edu.cn)

Abstract. Sea spray-mediated heat flux plays an important role in air-sea heat transfer. Heat flux integrated over droplet size spectrum can well simulate total heat flux induced by sea spray droplets. Previously, a fast algorithm of spray-flux assuming single-radius droplets (A15) was widely used since the full-size spectrum integral is computationally expensive. Based on the Gaussian Quadrature (GQ) method, a new fast algorithm (SPRAY-GQ) of sea spray-mediated heat flux is derived. The performance of SPRAY-GQ is evaluated by comparing heat fluxes with those estimated from the widely-used A15. The new algorithm shows a better agreement with the original spectrum integral. To further evaluate the numerical errors of A15 and SPRAY-GQ, the two algorithms are implemented into a coupled CFSv2.0-WW3 system, and a series of 56-day simulations in summer and winter are conducted and compared. The comparisons with satellite measurements and reanalysis data show that the SPRAY-GQ algorithm could lead to more reasonable simulation than the A15 algorithm by modifying air-sea heat flux. For experiments based on SPRAY-GQ, the sea surface temperature at mid-high latitudes of both hemispheres, particularly in summer, is significantly improved compared with the experiments based on A15. The simulation of 10-m wind speed and significant wave height at mid-low latitudes of the Northern Hemisphere after the first two weeks is improved as well. These improvements are due to the reduced numerical errors. The computational time of SPRAY-GQ is about the same as that of A15. Therefore~~Thereby~~, the newly-developed SPRAY-GQ algorithm has a potential to be used for calculation of spray-mediated heat flux in coupled models.

1 Introduction

Sea spray droplets, ejected from oceans, include film drops, jet drops and spume drops (Veron, 2015). The first two types of droplets are generated from bubble bursting caused by ocean surface wave breaking, with radius ranging from 0.5 μm to 50 μm (Resch and Afeti, 1991; Thorpe, 1992; Melville, 1996; Spiel, 1997; Andreas, 1998; Lhuissier and Villermaux, 2012). Spume drops are generated by strong winds (> 7-11 m/s) which directly tear the wave crests, with larger radius ranging from tens to hundreds of micrometers (Koga, 1981; Andreas et al., 1995; Andreas, 1998). Sea spray droplets play an important role in weather and climate processes (Fox-Kemper et al., 2022). On one hand, sea spray droplets contribute to local marine aerosols and subsequently modify the local radiation balance (Fairall et al., 1983; Burk, 1984; Fairall and Larsen, 1984). On the other hand, sea spray droplets affect the fluxes of heat, momentum, salt, and freshwater between atmosphere and ocean (Andreas, 1992; Andreas et al., 2008; Andreas, 2010; Andreas et al., 2015; Ling and Kao, 1976; Fairall et al., 1994; Andreas and Decosmo, 2002).

The sea spray-mediated heat transfer mainly occurs within the droplet evaporation layer (DEL) near the sea surface (Andreas and Decosmo, 1999, 2002; Fairall et al., 1994). Sea spray droplets with the same temperature as ocean surface can lead to sensible heat flux in DEL, while water evaporated from these droplets can further release latent heat to the atmosphere (Andreas, 1992; Borisenkov, 1974; Bortkovskii, 1973; Wu, 1974; Monahan and Van Patten, 1988; Ling and Kao, 1976). Part of the sea spray-mediated sensible heat is absorbed by droplet evaporation, which further increases the air-sea temperature difference, and thus increases the sea spray-mediated sensible heat flux (Fairall et al., 1994; Andreas and Decosmo, 2002). Since strong winds produce more sea spray droplets with larger radius, sea spray-mediated heat fluxes increase with wind speed (Fairall et al., 1994), and contribute to more than 10% of the total surface heat flux after reaching the threshold speed (> 11 m/s for sensible heat flux and > 13 m/s for latent heat flux)(Andreas et al., 2008). In addition, when a droplet is released into the air, it is accelerated due to surface winds (Edson and Andreas, 1997; Fairall et al., 1994; Van Eijk et al., 2011; Wu et al., 2017). If the droplet could fall back into the ocean, additional momentum would be injected into the ocean from the atmosphere (Andreas, 1992, 2004).

The usual bulk parameterizations in numerical models for surface fluxes only include the interfacial (turbulent) fluxes (e.g., Fairall et al., 1996), while neglecting the significant contributions of sea spray droplets in DEL (Andreas et al., 2008; Fairall et al., 1994; Smith, 1997; Emanuel, 1995). Andreas and Emanuel (2001) implemented sea spray-mediated heat flux and momentum flux parameterizations into a simple tropical cyclone model, and found that the sea spray-mediated heat flux can significantly enhance tropical cyclone intensity. ~~It is well known that strong winds and high waves induced by tropical cyclones can enhance sea surface roughness and thus surface drag coefficients. Although it is under debate whether the increased surface drag coefficients directly reduce tropical cyclone intensity (e.g., Emanuel, 1995; Smith et al., 2014), the increased momentum flux due to surface drag coefficients does enhance sea surface cooling and thus suppress tropical cyclone intensification (Liu et al., 2022)., which tend to reduce tropical cyclone intensity (Emanuel, 1995). Furthermore, the accelerated sea spray droplets by surface winds also lead to more dissipation of tropical cyclone kinetic energy (Andreas, 1992, 2004). These negative effects could be offset by the sea spray-mediated heat flux.~~ The similar enhancement of tropical cyclone intensity was also noticed in recent regional coupling systems by including sea spray-mediated heat flux (Xu et al., 2021a; Liu et al., 2012; Garg et al., 2018; Zhao et al., 2017). In the First Institute of Oceanography Earth System Model, Bao et al. (2020) first incorporated the sea spray-mediated heat flux in global climate simulation. Following Bao et al. (2020), Song et al. (2022) found that the sea spray-mediated heat flux can lead to cooling at the air-sea interface and westerlies strengthening ~~westerlies~~ in the Southern Ocean, and thus improves estimates of sea surface temperature (SST).

Since the parameterization of sea spray-mediated heat flux derived from observations requires full-size spectral integral and thus is computationally expensive for large-scale models (Table 1, details in Section 4.2; Andreas, 1989, 1990, 1992; Andreas et al., 2015), a simplified algorithm based on a single radius of sea spray droplets (Andreas et al., 2015; Andreas et al., 2008) is widely used in atmosphere-ocean coupling systems (Xu et al., 2021a; Liu et al., 2012; Garg et al., 2018; Zhao et al., 2017; Song et al., 2022; Bao et al., 2020), and apt to produce numerical errors. To reduce these numerical errors induced by the single radius of sea spray droplets, we develop a new fast algorithm of sea spray-mediated heat flux based on the Gaussian Quadrature (GQ) method, a fast and accurate way to calculate spectral integral. The GQ method has been successfully used for the estimation of domain-averaged radiative flux profiles

(Li and Barker, 2018). The performance of the GQ-based fast algorithm of the sea spray-mediated heat flux is evaluated and compared with the simplified algorithm for single radius of Andreas et al. (2015), referred to as A15 hereafter. The results are first compared with the original parameterization using full-size spectral integral (A92, hereafter). Then the parameterizations with different algorithms are implemented in a global coupled atmosphere-ocean-wave system (Shi et al., 2022), and the results are compared with global satellite measurements and reanalysis data.

The rest of the paper is structured as follows: observation and reanalysis data for comparisons are introduced in Section 2; the derivation of the GQ-based fast algorithm and the global coupling system are described in Section 3; the performance of the new fast algorithm is evaluated in Section 4. Finally, a summary and discussion are given in Section 5.

2 Data

The fifth generation European Centre for Medium-Range Weather Forecasts (ECMWF) Reanalysis (ERA5; Hersbach et al., 2020) 10-m wind speed (WSP10), 2-m air temperature (T02), 2-m dewpoint temperature, surface pressure and significant wave height (SWH) with a spatial resolution of 0.5° are used. Additionally, WSP10, T02 and 2-m specific humidity (SPH) data from the Objectively Analyzed air-sea Fluxes (OAFlux) products (Yu et al., 2008) are also applied for comparison, with 1°×1° resolution. The daily average satellite Optimum Interpolation SST (OISST) data are obtained from the National Oceanic and Atmospheric Administration (NOAA) with a spatial resolution of 0.25° (Reynolds et al., 2007). The global monthly mean salinity observations from European Space Agency (ESA; https://climate.esa.int/sites/default/files/SSS_cci-D1.1-URD-v1r4_signed-accepted.pdf) are applied. Besides, we also use the monthly global ocean RSS Satellite Data Products for WSP10 (https://data.remss.com/wind/monthly_1deg/) and the Reprocessed L4 Satellite Measurements for SWH (https://doi.org/10.48670/moi-00177), to validate the simulation results and ERA5 data.

3 Methods

3.1 Development of a Fast Algorithm Based on GQ

The effects of sea spray droplets on sensible and latent heat fluxes ($H_{S,SP}$, $H_{L,SP}$) contribute to the total turbulent sensible and latent heat fluxes ($H_{S,T}$, $H_{L,T}$) at the air-sea interface. That is,

$$H_{S,T} = H_S + H_{S,SP}, \quad (1)$$

$$H_{L,T} = H_L + H_{L,SP}. \quad (2)$$

where H_S and H_L are the sensible and latent heat fluxes at the air-sea interface due to the air-sea differences of temperature and humidity. Based on observations of total turbulent heat fluxes and the COARE algorithm (Andreas et al., 2015; Fairall et al., 1996), A92 integrates the sea spray-mediated sensible and latent heat flux spectrums over initial droplet radius ($Q_S(r_0)$ and $Q_L(r_0)$) to estimate $H_{S,SP}$ and $H_{L,SP}$ (details in Appendix A; Andreas, 1989, 1990, 1992; Andreas and Decosmo, 2002). The distributions of $Q_S(r_0)$ and $Q_L(r_0)$ spectrums as functions of initial droplet radius r_0 under various atmosphere and ocean states are shown in Fig. 1, indicating that Q_S and Q_L spectrums are more sensitive to the change of WSP10, and less sensitive to other variables, including T02, 2-m relative humidity, SST, surface air pressure and sea surface salinity.

Since t~~T~~he calculation of $H_{S,SP}$ and $H_{L,SP}$ in A92 is computationally expensive due to full-size spectral integral (Eqn. A5-A6 of Appendix A), ~~therefore~~ it is difficult to apply A92 directly in coupled modeling systems. A15 (Andreas et al., 2015) developed a fast algorithm by using a single representative droplet radius (details in Appendix B), which was widely adopted in recent regional and global coupling systems (Xu et al., 2021a; Liu et al., 2012; Garg et al., 2018; Zhao et al., 2017; Song et al., 2022; Bao et al., 2020). In this study, we apply a 3-node GQ method (details in Appendix C) to develop a new fast algorithm to approximate the full-size spectral integral of A92. Notably, GQ can converge exponentially to the actual integral only for a smooth function, which is a prerequisite for GQ (McClarren, 2018). Since as functions of r_0, $Q_S(r_0)$ and $Q_L(r_0)$ are not smooth (Fig. 1), a data sorting from largest to smallest is required. After sorting, local $Q_S(r_0)$ and $Q_L(r_0)$ become $Q_{S\_sort}(m)$ and $Q_{L\_sort}(m)$, and then GQ can be used to estimate the integral of $Q_{S\_sort}(m)$ and $Q_{L\_sort}(m)$. Note that the independent variable m is not equivalent to the original r_0, but only indicates the position. In this way, according to Appendix

C, m_1=443, m_2=251, m_3=58 are three GQ nodes of $Q_{S\_sort}(m)$ and $Q_{L\_sort}(m)$-, and we can get the corresponding r_0 for local Q_S (Q_L), denoted as r_{S1} (r_{L1}), r_{S2} (r_{L2}) and r_{S3} (r_{L3}). However, the sorting leads to high complexity of GQ comparable to A92, and the values of r_{S1} (r_{L1}), r_{S2} (r_{L2}) and r_{S3} (r_{L3}) vary under various atmosphere and ocean statesenvironments in the globe. Therefore, it is necessary to find the general approximate values of r_{S1} (r_{L1}), r_{S2} (r_{L2}) and r_{S3} (r_{L3}) via global statistical analyses, to avoid the sorting in application.

To derive the general approximate values of r_{S1} (r_{L1}), r_{S2} (r_{L2}) and r_{S3} (r_{L3}), we calculate the distribution of the sea spray-mediated heat flux spectral following A92, based on the global daily WSP10, T02, 2-m dewpoint temperature, surface pressure and SWH of ERA5 and OISST from August 1, 2018 to August 31, 2018. Since the sea spray-mediated heat flux is not sensitive to salinity (Fig. 1e&f) and only monthly observational data is available, the ESA monthly salinity is applied. From the global spectrums, we sort Q_S and Q_L from largest to smallest to obtain local r_{S1}, r_{S2} and r_{S3} (r_{L1}, r_{L2} and r_{L3}) for every grid point, whose global distribution of occurrence frequency in percentage is shown in Fig. 2. It is noted that except for r_{L3}, all other five nodes have frequency roughly concentrated at a constant (peak frequency >65% in Fig. 2a, b, d-f; Eqn. 3&4), while for r_{L3}, there is a 92.53% concentration between 55 and 90 μm (Fig. 2c). Then we found that r_{L3} (55-90 μm) is related to WSP10 (Fig. S1 in supplementary), thereby we set the approximate values as

$$r_{S1} = 459.056,\ r_{S2} = 294.185,\ r_{S3} = 166.771, \tag{3}$$

$$r_{L1} = 443.914, r_{L2} = 251.0498, \tag{4}$$

$$r_{L3} = \begin{cases} 60.310\text{WSP10}^{0.1161}, & \text{WSP10} \geq 2\ m/s \\ 58.086, & \text{WSP10} < 2\ m/s \end{cases}, \tag{5}$$

where the unit of the radius is micrometer. Afterwards, we directly use Eqn. 3-5 to approximate the full-size spectral integral of A92 without sorting as

$$\int_a^b Q_S(r_0)dr_0 \approx \frac{b-a}{2}\sum_{i=1}^{3}\omega_i Q_S(r_{Si}), \tag{6}$$

$$\int_a^b Q_L(r_0)dr_0 \approx \frac{b-a}{2}\sum_{i=1}^{3}\omega_i Q_L(r_{Li}). \tag{7}$$

Here a and b are the lower and upper limits of r_0, which are set to $2\mu m$ and $500\mu m$ based on Andreas (1990), and ω_i is the corresponding weight (ω_1=ω_3=0.556, ω_2=0.889), obtained from McClarren

(2018). The new fast algorithm for approximations of $H_{S,SP}$ and $H_{L,SP}$ is referred to as SPRAY-GQ hereafter.

3.2 CFSv2.0-WW3 Coupling System

A coupled system based on Climate Forecast System model version 2.0 (CFSv2.0) and WAVEWATCH III (WW3) is employed to evaluate and compare the effects of sea spray-mediated heat flux parameterized by A15 and SPRAY-GQ. The CFSv2.0-WW3 has three components, the Global Forecast System (GFS; http://www.emc.ncep.noaa.gov/GFS/doc.php) as the atmosphere component of CFSv2.0, the Modular Ocean Model version 4 (MOM4; Griffies et al., 2004) as the ocean component of CFSv2.0, and the WW3 (WAVEWATCH III Development Group, 2016) as the ocean surface wave component. The variables between CFSv2.0 and WW3 are interpolated and passed using the Chinese Community Coupler version 2.0 (C-Coupler2; Liu et al., 2018).

The CFSv2.0 is mainly applied for intraseasonal and seasonal prediction (e.g., Saha et al., 2014). The atmosphere component GFS uses a spectral triangular truncation of 382 waves (T382) in the horizontal, equivalent to a grid resolution of nearly 35 km, and 64 sigma-pressure hybrid layers in the vertical. The MOM4 is integrated on a nominal 0.5° horizontal grid with enhanced horizontal resolution to 0.25° in the tropics, and there are 40 levels in the vertical. The CFSv2.0 initial fields at 00:00 UTC of the first day for experiments were generated by the real time operational Climate Data Assimilation System (Kalnay et al., 1996), downloaded from the CFSv2.0 official website (http://nomads.ncep.noaa.gov/pub/data/nccf/com/cfs/prod). The latitude range of WW3 is 78°S–78°N with a spatial resolution of 1/3°. The initial wave fields were generated from 10-day simulations starting from rest in a stand-alone WW3 model, forced by ERA5 10-m winds and ice concentration. The open boundary conditions of WW3 were also obtained by the global simulation of the stand-alone WW3 model.

In the coupling system, the WW3 obtains 10-m wind and ocean surface current from CFSv2.0, and then provides wave parameters to CFSv2.0. Several wave-mediated processes, including upper ocean mixing modified by Stokes drift-related processes, air-sea fluxes modified by surface current and Stokes drift, and momentum roughness length, are considered. Details of this system are referred to Shi et al. (2022).

A series of numerical experiments is conducted to evaluate the effects of the two fast algorithms (A15 and SPRAY-GQ) of sea spray-mediated heat flux on ocean, atmosphere and waves in two 56-day periods, from January 3 to February 28, 2017 and from August 3 to September 28, 2018 for boreal winter and boreal summer, respectively. For each period, two sensitivity experiments are carried out. The first is the SPRAY-A15 experiment, in which A15 is used with two-way fully coupling. The second is the SPRAY-GQ experiment, in which SPRAY-GQ fast algorithm is used instead of A15. In addition, we also carry out another 7-day experiment using A92 (SPRAY-A92) to test the runtime.

4 Results

4.1 Comparison with A92

Based on the daily global WSP10, T02, 2-m dewpoint temperature, surface pressure and SWH of ERA5, the daily global OISST, and the ESA monthly global salinity, $H_{S,SP}$ and $H_{L,SP}$ from A15, SPRAY-GQ and A92 are calculated (Fig. 3). The computational time for SPRAY-GQ is about the same as that for A15, and about 36 times less than the time for A92. Compared with A92 (the black dotted line), A15 (red) overestimates $H_{S,SP}$ for low $H_{S,SP}$ (<50 W/m^2) and underestimates $H_{S,SP}$ for high $H_{S,SP}$ (>50 W/m^2) with a root mean square error (RMSE=$\sqrt{\sum_{i=1}^{n}(\hat{y_i}-y_i)^2/n}$, $\hat{y_i}$ is A15 value, y_i is A92 value, and *n* is the total number of grid points) of 3.40 W/m^2 (Fig. 3a), while A15 shows consistent overestimations with a RMSE of 2.98 W/m^2 for $H_{L,SP}$ (Fig. 3b). Overall, the RMSE of A15 is about 2.69 W/m^2 for sea-spray mediated total heat flux ($TH_{SP} = H_{S,SP}$+$H_{L,SP}$; Fig. 3c). Andreas et al. (2015) derived A15 from A92 using single-radius droplets as bellwethers and wind functions, and extrapolated the wind functions at high wind speeds >25 m/s. Since the wind speeds in the study are less than 25 m/s (Fig. S1), the large difference between A15 and A92 is mainly due to the use of single-radius droplets. Compared with A15, SPRAY-GQ (blue) has less deviation from A92 for both $H_{S,SP}$ and $H_{L,SP}$ (Fig. 3a&b). The corresponding RMSEs of SPRAY-GQ for $H_{S,SP}$, $H_{L,SP}$ and TH_{SP} are 0.83 W/m^2, 0.92 W/m^2 and 0.62 W/m^2, all significantly lower (P<0.05 in Student's t-test) than those of A15.

To test robustness of the results, we also use WSP10, T02 and SPH of OAFlux dataset to estimate $H_{S,SP}$ and $H_{L,SP}$. As shown in Fig. 4, SPRAY-GQ has significantly (P<0.05 in Student's t-test) lower deviations and RMSEs than A15, consistent with Fig. 3. Note that the values of $H_{S,SP}$ and $H_{L,SP}$ in Fig.4 are larger than those in Fig. 3. It is because OAFlux only provides neutral wind speeds, calculated from wind stress and the corresponding roughness by assuming air is neutrally stratified. The neutral winds from OAFlux are larger than winds in ERA5 as indicated by previous studies (Lindemann et al., 2021; Seethala et al., 2021).

In addition, since it is common to derive SWH from empirical equations (e.g., Andreas et al., 2008; Andreas et al., 2015; Andreas and Decosmo, 2002; Andreas, 1992), we also use SWH generated by empirical equations of WSP10 (Andreas, 1992) instead of ERA5 SWH to estimate $H_{S,SP}$ and $H_{L,SP}$ (Fig. 5). Again, the RMSEs decrease significantly ($P<0.05$ in Student's t-test) in SPRAY-GQ compared to A15, though the RMSEs become higher for all estimates due to the enhanced biases of SWH. The difference between SPRAY-GQ and A92 is always smaller than that between A15 and A92. Next, we will evaluate and compare the two fast algorithms in an atmosphere-ocean-wave coupled system (CFSv2.0-WW3).

4.2 Comparison in the CFSv2.0-WW3 Coupling System

To compare the computational time of different parameterizations in the large-scale modeling system, the runtime of the fully coupled experiments for 7-day forecast is given in Table 1 as an example. It is shown that the runtime is about the same for SPRAY-GQ and SPRAY-A15. Both experiments run about 17 times faster than SPRAY-A92.

To illustrate the numerical errors of the two fast algorithms discussed in the context of the coupled system, comparisons are made for simulated SSTs, WSP10s as well as SWHs against OISST and ERA5 reanalysis. The results in the first three days are excluded in the comparison, since the wave influences are weak at the beginning of the simulations. Overall, the WSP10s of simulations are generally in the range of 0-25 m/s globally. At mid-high latitudes, the WSP10s generally exceed 10 m/s (Fig. S2&S3 of the supplementary), at which the effects of sea spray can become significant (Andreas et al., 2015; Andreas et al., 2008).

4.2.1 Sea Surface Temperature (SST)

In the austral summer, compared with OISST, large SST biases (>1 ℃ or <-1 ℃) of SPRAY-A15 occur in the Southern Hemisphere (SH; Fig. S4a in supplementary), especially in the Southern Ocean. It is always a challenge ~~for~~ to ~~reducing~~ reduce the large SST biases in the Southern Ocean for climate models (e.g., Alessandro et al., 2019; Wang et al., 2014; Li et al., 2013; Bodas-Salcedo et al., 2012; Ceppi et al., 2012). In Fig. 6a, SSTs north (south) of 50°S in experiment SPRAY-A15 are mainly underestimated (overestimated). The domain-averaged RMSE (0-360°E, 40-75°S) in experiment SPRAY-A15 increases in the first month and then levels off (red solid line in Fig. 6c),~~.~~ w~~W~~hile the domain-averaged RMSE in experiment SPRAY-GQ levels off about a week earlier (black solid line in Fig. 6c). The mean RMSE in SPRAY-GQ is significantly lower than that in SPRAY-A15 (P<0.05 in Student's t-test). The increased (decreased) SSTs north (south) of 50°S in SPRAY-GQ compared to those in SPRAY-A15 (Fig. 6b) reduce the RMSE of SST in SPRAY-GQ. We also calculate the mean absolute error, MAE=$\sum_{i=1}^{n}|\hat{y}_i - y_i|/n$, where $\hat{y}_i$ is simulated value and y_i is OISST data, and *n* is the total number of grid points. The MAEs are consistent with RMSEs (dotted line in Fig. 6c). Furthermore, the mean errors, ME=$\sum_{i=1}^{n}(\hat{y}_i - y_i)/n$ (Fig. S5a in the supplementary), are smaller in SPRAY-GQ than SPRAY-A15.

To understand the effects of sea spray droplets on SST, we calculate the total heat flux (TH=$H_{S,T}$+$H_{L,T}$) differences between SPRAY-GQ and SPRAY-A15 (Fig. 7a). The TH differences are significantly correlated with SST differences (Fig. S4b in the supplementary), with the spatial correlation coefficient of -0.41 (P<0.05 in Student's t-test). We further decompose direct and indirect effects of sea spray droplets on heat fluxes following Song et al. (2022). The direct effect ($H_{S,SP}$ and $H_{L,SP}$) is induced directly by sea spray droplets, calculated from A15 (Eqn. B1-B4 of Appendix B) and SPRAY-GQ (Section 3.1). The indirect effect (H_S and H_L) is the heat flux variation induced by changes of atmosphere and ocean variables (including wind, pressure, humidity and temperature) caused by direct effect, estimated by subtracting $H_{S,SP}$ and $H_{L,SP}$ from the output heat fluxes ($H_{S,T}$ and $H_{L,T}$) of experiment SPRAY-A15 and SPRAY-GQ.

In the Southern Ocean, although direct differences of $H_{S,SP}$ and $H_{L,SP}$ are relatively small (<10 W/m^2, Fig. 7b, e, &h), the resulting changes of temperature and humidity lead to relatively large differences in indirect effects of H_S and H_L (Fig. 7c, f, &i). Enhanced (reduced) TH_{SP} from ocean to atmosphere in the summer leads to increased (decreased) air-sea temperature difference and thus enhances (weakens) H_S. Meanwhile the warmer (cooler) air also causes more (less) evaporation and thus more (less) H_L. Finally, the enhanced (reduced) TH cools (warms) SST.

In the boreal summer, large SST biases (>1 °C or <-1 °C) of SPRAY-A15 mainly occur at mid-high latitudes of the Northern Hemisphere (NH; Fig. S6a in supplementary). Significant underestimations occur in the western and northern part of the North Pacific and at mid latitudes of the North Atlantic, while large positive SST biases mainly occur in the eastern part of the North Pacific and at high latitudes of the North Atlantic (Fig. 8a). In experiment SPRAY-GQ, SSTs are warmer (cooler) in the previously underestimated (overestimated) regions (Fig. 8b). Therefore, the domain-averaged RMSE and MAE (0-360°E, 20-75°N) in SPRAY-GQ are significantly lower (P<0.01 in Student's t-test) than in SPRAY-A15 after the first three weeks (Fig. 8c). Compared to SPRAY-A15, the overall underestimation is reduced in SPRAY-GQ (Fig. S5b). The spatial correlation coefficient between TH differences and SST differences (Fig. 9a&Fig. S6b) is -0.32 (P<0.05 in Student's t-test). Consistent with the austral summer, the SST changes are related to the changes of heat flux (Fig. 9). The indirect effects of latent heat flux (Fig. 9f) play a major role in TH differences, which are modified by the direct effects (Fig. 9b, e, &h). In addition, the changes of surface wind also contribute to the changes of SST. The reduced winds weaken the upper ocean mixing, the water becomes more stratified, and then the SST tends to be warmer, and vice versa (Fig. S7&S8).

4.2.2 10-m Wind Speed (WSP10) and Significant Wave Height (SWH)

Compared with experiment SPRAY-A15, significant differences of WSP10 in SPRAY-GQ occur at mid-low latitudes of the NH (0-360°E, 0-60°N) in both winter and summer (Fig.S7b&S8b). As we know, satellite scatterometer and altimeter data are usually used to validate WSP10 and SWH for short term weather forecast (e.g., Accadia et al., 2007; Djurdjevic and Rajkovic, 2008; Myslenkov et al., 2021). However, due to the spatial and temporal coverage of satellite data, we can only obtain the monthly averaged satellite data for the globe. ~~So~~ Therefore, we compare the monthly averaged WSP10 and SWH from simulations with the corresponding satellite data (Fig. S9-S12). The comparison results (Fig.

S9a&c-S12a&c) are consistent with those compared with ERA5 (Fig. S9b&d-S12b&d). From Fig. S9e-S12e, the differences of WSP10s between ERA5 and the satellite data are always less than 1 m/s and the differences of SWHs are always less than 0.3 m. Since ERA5 provides daily data for comparison, we will use ERA5 for validation in the following.

The ME of WSP10 (SPRAY-A15 minus ERA5) is 0.28 m/s and 0.47 m/s in winter and summer (red in Fig. S5c&d), respectively, mainly due to the overestimations over the Pacific and the Atlantic Ocean (red in Fig.10a&11a). Whereas in SPRAY-GQ, the ME (SPRAY-GQ minus ERA5) is 0.15 m/s and 0.33 m/s in winter and summer respectively (black in Fig. S5c&d). The domain-averaged RMSEs and MAEs of WSP10s increase with time in the first two weeks and then gradually level off (Fig. 10c&11c). The differences of WSP10 RMSEs and MAEs between SPRAY-GQ (black) and SPRAY-A15 (red) are very small in the first two weeks. Afterwards the mean values of RMSE and MAE in SPRAY-GQ are lower than those in SPRAY-A15 significantly at 95% confidence level in both boreal winter (Fig. 10c) and boreal summer (Fig. 11c).

The simulated SWHs changes are closely related to the changes of WSP10s (Shi et al., 2022). Therefore, the differences of SWHs (Fig.12&13) are consistent with those of WSP10s (Fig.10&11), with overestimated (underestimated) WSP10s corresponding to overestimated (underestimated) SWHs compared with ERA5. The SWHs in SPRAY-GQ are significantly different ~~with~~ from those in SPRAY-A15 (Fig. 12b&13b). In winter (summer), the SWH RMSE averages for SPRAY-A15 and SPRAY-GQ are 1.31 m (0.98 m) and 1.23 m (0.87 m), and after the first two weeks the RMSE and MAE in SPRAY-GQ are lower than those in SPRAY-A15 significantly at 95% confidence level in both winter (Fig. 12c) and summer (Fig. 13c).

The direct and indirect effects of sea spray droplets on heat fluxes can influence estimates of WSP10 and then SWH. The changes of WSP10s are related to the direct effects ($H_{S,SP}$ and $H_{L,SP}$; Fig. 7b, e, &h; Fig. 9b, e, &h). The spatial correlation coefficients between WSP10 differences (Fig. S7b&S8b) and TH_{SP} differences (Fig. 7b&9b) are 0.51 and 0.69 (P<0.01 in Student's t-test) in winter and summer, respectively,~~.~~ b~~B~~ecause TH_{SP} differences can influence the sea level pressure (SLP) distribution (Fig. S15&S16), and subsequently surface winds. For example, compared with SPRAY-A15, the decreased TH_{SP} of SPRAY-GQ in the Northwest Pacific in summer (Fig. 9b) leads to higher SLP and smaller pressure gradient (Fig. S16), and thus decreased WSP10 (Fig. 11b); while the increased TH_{SP} in the Gulf of Alaska (Fig. 9b) leads to lower SLP and larger pressure gradient (Fig. S16), and thus enhanced WSP10 (Fig. 11b). The accelerated (decelerated) WSP10s further result in increased (decreased) interfacial heat transport (H_S, H_L), as well as increased (decreased) SWHs.

5 Conclusions and Discussion

Based on a GQ method, we develop a new fast algorithm based on Andreas's (1989, 1990, 1992) full-size microphysical parameterization (A92) for sea spray-mediated heat fluxes. Using global satellite measurements and reanalysis data, we found that the difference between SPRAY-GQ and A92 is significantly smaller than that between A15 and A92 (Andreas et al., 2015). To evaluate the numerical error of SPRAY-GQ/A15 fast algorithm, we implement them in the two-way coupled CFSv2.0-WW3 system. A series of 56-day simulations from January 3 to February 28, 2017 and from August 3 to September 28, 2018 are conducted. The results are compared against satellite measurements and ERA5 reanalysis. The comparison shows that the sea spray-mediated heat flux in SPRAY-GQ can reasonably modulate total heat flux compared with SPRAY-A15, and significantly reduce the SST biases in the Southern Ocean (mid-high latitudes of the NH) for the austral (boreal) summer, as well as WSP10 and SWH after the first two weeks at mid-low latitudes of the NH for both boreal winter and summer. Overall, our fast algorithm based on GQ is applicable to sea spray-mediated heat flux parameterization in coupled models.

To investigate the effects of spray-mediated heat flux on simulations, two 56-day experiments without sea spray effect (CTRL) in boreal winter and summer ~~respectively~~ are conducted respectively, and the differences of simulated SST, WSP10, SWH, T02 and SPH between SPRAY-GQ and CTRL are compared in Fig. S17-S21 in the supplementary. The introduction of sea spray cannot significantly reduce the global overall errors of simulations, but it leads to regional improvements (blue in Fig. S17e&f-S21e&f). For example, compared with CTRL in Jan-Feb, 2017, SST MAE of SPRAY-GQ in the southeast of Australia decreases (Fig. S17e), because of warmer SST (Fig. S17c) related to reduced wind (Fig. S18c). The reduced wind here also leads to lower SWH (Fig. S19c) and thus reduced SWH overestimation (Fig. S19e). Meanwhile, SPRAY-GQ reduces MAE of T02 and SPH (Fig. S20e&S21e)

by increasing temperature and moisture (Fig. S20c&S21c). The reduced errors are related to the relatively large WSP10s over the areas (Fig. S2&S3), since the effects of sea spray become important at wind speeds larger than 10 m/s.

In addition to the variables aforementioned, the changes of simulated cloud fraction were also compared. However, the effects of sea spray-mediated heat flux on cloud fraction are non-significant for the 2-month simulation, so the results are not shown. Besides, the lack of other processes related to sea spray may be one of the reasons why the global overall error cannot be reduced effectively. For example, for simulated WSP10 and SWH in SPRAY-GQ, the significant overestimations in the SH still exist especially in Aug-Sep, 2018 (Fig. S18&S19 in supplementary). As Andreas (2004) indicated, sea spray droplets also influence the surface momentum flux by injecting more momentum into the ocean from the atmosphere, which might further decrease the surface wind speed. We will consider this process in the future study.

Sea spray-mediated heat fluxes are related to the sea spray generation function (SSGF). Based on a number of laboratory and field observations, varieties of SSGF were derived (e.g., Koga, 1981; Monahan et al., 1982; Troitskaya et al., 2018; Andreas, 1992, 1998, 2002; Fairall et al., 1994; Veron, 2015), whereas their differences can reach six orders of magnitude (Andreas, 1998). There is currently no consensus on the most suitable choice. In this study, we use SSGF of Fairall et al. (1994), recommended by Andreas (2002), to get a mean bias of 3.70 W/m^2 and 0.095 W/m^2 for latent and sensible heat flux respectively (Andreas et al., 2015), consistent with recent observations of Xu et al. (2021b). ~~Even though~~However, the improved SST and other variables cannot be reliably assigned to the usage of the GQ method, due to the uncertainties of the coupled model itself and SSGF.

When wind speed is larger than 10 m/s, spray-mediated heat flux can become as important as the interfacial heat flux (Andreas and Decosmo, 1999, 2002). Particularly, even in the absence of air-sea temperature difference, the spray-mediated sensible heat flux is still present (Andreas et al., 2008). As indicated by previous studies (e.g., Garg et al., 2018; Song et al. 2022), it is necessary to superimpose the spray-mediated heat flux on the bulk formula to complete the physics of turbulent heat transfer for coupled simulation. Since the full microphysical parameterization (A92) is computationally expensive, an efficient algorithm that captures the main features of A92 can be beneficial to large-scale climate systems or operational storm models. The GQ method proposed in the study can efficiently calculate the spray-mediated heat flux, and agree better with A92 than A15. ~~Thereby~~Therefore, the GQ based spray-mediated heat flux is promising to be widely applied in large-scale climate systems and operational storm models.

Appendix A

Microphysical Parameterization of A92

Based on the cloud microphysical parameterization of Pruppacher and Klett (1978), Andreas (1989, 1990, 1992) proposed a parameterization of sea spray-related heat fluxes for droplets with different radius, from formation at sea surface to equilibrium with environment, that is,

$$Q_S = \rho_w C_{ps}\left(T_w - T_{eq}\right)\left[1 - \exp\left(-\frac{\tau_f}{\tau_T}\right)\right]\left(\frac{4\pi r_0^3}{3}\frac{dF}{dr_0}\right), \qquad \text{(A1)}$$

$$Q_L = \begin{cases} \rho_w L_v\left\{1 - [\frac{r(\tau_f)}{r_0}]^3\right\}\left(\frac{4\pi r_0^3}{3}\frac{dF}{dr_0}\right), \tau_f \le \tau_r, \\ \rho_w L_v\left\{1 - (\frac{r_{eq}}{r_0})^3\right\}\left(\frac{4\pi r_0^3}{3}\frac{dF}{dr_0}\right), \tau_f > \tau_r. \end{cases} \qquad \text{(A2)}$$

Here Q_S, Q_L are sensible heat flux and latent heat flux resulted ~~by~~ from sea spray droplets with initial radius r_0, ρ_w is the sea water density, C_{ps} is the specific heat, L_v is the latent heat of vaporization of water, T_w is the water temperature, T_{eq} is the temperature of droplet when it reaches thermal equilibrium with ambient condition, r_{eq} is the radius of droplet when it reaches moisture equilibrium with ambient condition, τ_f is the residence time for droplets in the atmospheric, $r(\tau_f)$ is the corresponding radius, τ_T is the characteristic e-folding time of droplet temperature, and τ_r is the characteristic e-folding time of droplet radius. The detailed calculation of these microphysical quantities can be found in Andreas (1989, 1990, 1992). ~~And~~ dF/dr_0 is the sea spray generation function, which represents the produced number ~~produced~~ of droplets with initial radius r_0 (Andreas, 1992). For this term, the function of Fairall et al. (1994) was recommended by Andreas (2002). According to the review in Andreas (2002), the dF/dr_0 of Fairall et al. (1994) is related on that of Andreas (1992) as

$$\frac{dF}{dr_0} = 38 \times 3.84 \times 10^{-6} U_{10}^{3.41} r_0^{-0.024} \frac{dF_{A92}}{dr_{80}}\bigg|_{U_{10}=11\,m/s}, \qquad \text{(A3)}$$

$$\left.\frac{dF_{A92}}{dr_{80}}\right|_{U_{10}=11\,m/s} = \begin{cases} e^{\left(4.405-2.646(logr_{80})-3.156(logr_{80})^2+8.902(logr_{80})^3-4.482(logr_{80})^4\right)}, r_{80}\le 15\mu m; \\ 1.02\times10^4 r_{80}^{-1}, 15\le r_{80}\le 37.5\mu m; \\ 6.95\times10^6 r_{80}^{-2.8}, 37.5\le r_{80}\le 100\mu m; \\ 1.75\times10^{17} r_{80}^{-8}, r_{80}\ge 100\mu m \end{cases}. \quad \text{(A4)}$$

Here U_{10} is the 10-m wind, $r_{80} = 0.518r_0^{0.976}$.

The total sea spray fluxes are obtained by integrating Q_S and Q_L corresponding to all r_0. Based on Andreas (1990), the lower and upper limits of r_0 is $2\mu m$ and $500\mu m$, that is,

$$\overline{Q_S} = \int_2^{500} Q_S(r_0)dr, \quad \text{(A5)}$$

$$\overline{Q_L} = \int_2^{500} Q_L(r_0)dr. \quad \text{(A6)}$$

~~While~~ Note that $\overline{Q_S}$ and $\overline{Q_L}$ are nominal sea spray fluxes but not the actual $H_{S,SP}$ and $H_{L,SP}$ (Andreas and Decosmo, 1999, 2002), because there are interactions between these two terms and the microphysical functions also lead to uncertainties (Fairall et al., 1994). Therefore, $\overline{Q_S}$ and $\overline{Q_L}$ are tuned by non-negative constants α, β and γ (Andreas and Decosmo, 2002; Andreas et al., 2008; Andreas et al., 2015; Andreas, 2003) as

$$H_{S,SP} = \beta\overline{Q_S} - (\alpha - \gamma)\overline{Q_L}, \quad \text{(A7)}$$

$$H_{L,SP} = \alpha\overline{Q_L}. \quad \text{(A8)}$$

In Eqn. (A8), the α term indicates the sea spray-mediated latent heat flux from the top of DEL to atmosphere. Because the evaporation of droplets absorbs heat, which is provided by sea spray-mediated sensible heat (Fairall et al., 1994), the negative α term appears in Eqn. (A7). ~~Whereas t~~The evaporation also cools DEL and thus increases the air-sea temperature difference, therefore it contributes to a positive γ term in Eqn. (A7). Different values of α, β and γ were given in Andreas and Decosmo (2002), Andreas (2003), Andreas et al. (2008) and Andreas et al. (2015), to minimize the bias between estimations and observations of turbulent heat fluxes measured by eddy correlation. And Andreas et al. (2015) validated the most observation data, which are 4000 sets, to derive $\alpha = 2.46, \beta = 15.15, \gamma = 1.77$.

Appendix B

Fast Algorithm of A15

Andreas (2003) and Andreas et al. (2008, 2015) developed a fast algorithm to approximate $H_{S,SP}$, $H_{L,SP}$ by a characteristic radius, that is,

$$H_{S,SP} = \beta\overline{Q_S} - (\alpha - \gamma)\overline{Q_L} \approx \rho_w C_{ps}\big(T_W - T_{eq,100}\big)V_s(u_*), \tag{B1}$$

$$H_{L,SP} = \alpha\overline{Q_L} \approx \rho_w L_v\left\{1 - [\frac{r(\tau_{f,50})}{50\mu\text{m}}]^3\right\}V_L(u_*). \tag{B2}$$

Here $T_{eq,100}$ is T_{eq} of droplets with r_0=100 μm, $\tau_{f,50}$ is τ_f of droplets with r_0=50 μm, V_s and V_L are functions of the bulk friction velocity u_*. As indicated by Andreas et al. (2008, 2015), the characteristic radiuses of 100 μm and 50 μm for sensible and latent heat fluxes are chosen, respectively, because Q_S and Q_L show a large peak in the vicinity of these values (Fig. 1). V_s and V_L are calculated in Andreas et al. (2015) as

$$V_S = \begin{cases} 3.92 \times 10^{-8}, & 0 \le u_* \le 0.1480\, m/s \\ 5.02 \times 10^{-6}u_*^{2.54}, & u_* \ge 0.1480\, m/s \end{cases}, \tag{B3}$$

$$V_L = \begin{cases} 1.76 \times 10^{-9}, & 0 \le u_* \le 0.1358\, m/s \\ 2.08 \times 10^{-7}u_*^{2.39}, & u_* \ge 0.1358\, m/s \end{cases}. \tag{B4}$$

Appendix C

Gaussian Quadrature (GQ)

GQ is a method to approximate the definite integral of a function $f(x)$ via the function values at a small number of specified nodes (Gauss, 1815; Jacobi, 1826). In this study we use the form of n-node Gauss–Legendre quadrature on [-1, 1] as

$$\int_{-1}^{1} f(x)dx \approx \sum_{i=1}^{n} \omega_i f(x_i). \tag{C1}$$

Here x_i is the specified node, and ω_i is the corresponding weight. For n=3, x_1=-0.775, x_2=0, x_3=0.775, ω_1=ω_3=0.556, ω_2=0.889.

~~While f~~For a function $g(\xi)$ on [a, b], Eqn. (C1) can be transformed to

$$\int_a^b g(\xi)d\xi = \int_{-1}^{1} g\left(\frac{b-a}{2}x + \frac{a+b}{2}\right)\frac{d\xi}{dx}dx \approx \frac{b-a}{2}\sum_{i=1}^{n}\omega_i g\left(\frac{b-a}{2}x_i + \frac{a+b}{2}\right). \tag{C2}$$

Code and data availability

The code of sea spray can be found under https://doi.org/10.5281/zenodo.7100345 or https://zenodo.org/record/7100345#.Y66vRtVByHt (Shi and Xu, 2022). The code for CFSv2.0-WW3 system can be found under https://doi.org/10.5281/zenodo.5811002 (Shi et al., 2021) including the coupling, preprocessing, run control and postprocessing scripts. The initial fields for CFSv2.0 are generated by the real time operational Climate Data Assimilation System, downloaded from the CFSv2.0 official website (http://nomads.ncep.noaa.gov/pub/data/nccf/com/cfs/prod). The daily average satellite Optimum Interpolation SST (OISST) data are obtained from NOAA (https://www.ncdc.noaa.gov/oisst). The fifth generation European Centre for Medium-Range Weather Forecasts (ECMWF) Reanalysis (ERA5) are available at the Copernicus Climate Change Service (C3S) Climate Date Store (https://cds.climate.copernicus.eu/cdsapp#!/dataset/reanalysis-era5-single-levels). The daily Objectively Analyzed air-sea Fluxes (OAFlux) products are available at https://oaflux.whoi.edu/heat-flux. The global monthly mean salinity observations of European Space Agency (ESA) are from https://climate.esa.int. The monthly global ocean RSS Satellite Data Products for 10-m wind speed are from https://data.remss.com/wind/monthly_1deg/, and the Reprocessed L4 Satellite Measurements for significant wave height are from https://doi.org/10.48670/moi-00177.

Author contribution

FX and RS designed the experiments and RS carried them out. RS developed the code of coupling parametrizations and produced the figures. RS prepared the manuscript with contributions from all co-authors. FX contributed to review and editing.

Acknowledgments

This work was supported by the National Key Research and Development Program of China (2020YFA0607900, 2021YFC3101601), and the National Natural Science Foundation of China (42176019). We thank Dr. Jiangnan Li for help of GQ codes. We also thank two anonymous reviewers and the handling editor for their constructive comments.

Competing Interests

The contact author has declared that neither they nor their co-authors have any competing interests.

References

Accadia, C., Zecchetto, S., Lavagnini, A., and Speranza, A.: Comparison of 10-m wind forecasts from a regional area model and QuikSCAT scatterometer wind observations over the Mediterranean Sea, Mon. Weather Rev., 135, 1945-1960, 2007.

Alessandro, J. D., Diao, M., Wu, C., Liu, X., Jensen, J. B., and Stephens, B. B.: Cloud phase and relative humidity distributions over the Southern Ocean in austral summer based on in situ observations and CAM5 simulations, Journal of Climate, 32, 2781-2805, 2019.

Andreas, E. L.: Thermal and size evolution of sea spray droplets, 1989.

Andreas, E. L.: Time constants for the evolution of sea spray droplets, Tellus B, 42, 481-497, 1990.

Andreas, E. L.: Sea spray and the turbulent air - sea heat fluxes, Journal of Geophysical Research: Oceans, 97, 11429-11441, 1992.

Andreas, E. L., Edson, J. B., Monahan, E. C., Rouault, M. P., and Smith, S. D.: The spray contribution to net evaporation from the sea: A review of recent progress, Boundary-Layer Meteorology, 72, 3-52, 1995.

Andreas, E. L.: A new sea spray generation function for wind speeds up to 32 ms− 1, Journal of Physical Oceanography, 28, 2175-2184, 1998.

Andreas, E. L., and Decosmo, J.: Sea spray production and influence on air-sea heat and moisture fluxes over the open ocean, in: Air-sea exchange: physics, chemistry and dynamics, Springer, 327-362, 1999.

Andreas, E. L., and Emanuel, K. A.: Effects of sea spray on tropical cyclone intensity, Journal of the atmospheric sciences, 58, 3741-3751, 2001.

Andreas, E. L.: A review of the sea spray generation function for the open ocean, Advances in Fluid Mechanics, 33, 1-46, 2002.

Andreas, E. L., and Decosmo, J.: The signature of sea spray in the HEXOS turbulent heat flux data, Boundary-layer meteorology, 103, 303-333, 2002.

Andreas, E. L.: 3.4 AN ALGORITHM TO PREDICT THE TURBULENT AIR-SEA FLUXES IN HIGH-WIND, SPRAY CONDITIONS, 2003.

Andreas, E. L.: Spray stress revisited, Journal of physical oceanography, 34, 1429-1440, 2004.

Andreas, E. L., Persson, P. O. G., and Hare, J. E.: A bulk turbulent air–sea flux algorithm for high-wind, spray conditions, Journal of Physical Oceanography, 38, 1581-1596, 2008.

Andreas, E. L.: Spray-mediated enthalpy flux to the atmosphere and salt flux to the ocean in high winds, Journal of physical oceanography, 40, 608-619, 2010.

Andreas, E. L., Mahrt, L., and Vickers, D.: An improved bulk air – sea surface flux algorithm, including spray - mediated transfer, Quarterly Journal of the Royal Meteorological Society, 141, 642-654, 2015.

Bao, Y., Song, Z., and Qiao, F.: FIO - ESM version 2.0: Model description and evaluation, Journal of Geophysical Research: Oceans, 125, e2019JC016036, 2020.

Bodas-Salcedo, A., Williams, K., Field, P., and Lock, A.: The surface downwelling solar radiation surplus over the Southern Ocean in the Met Office model: The role of midlatitude cyclone clouds, Journal of Climate, 25, 7467-7486, 2012.

Borisenkov, E.: Some mechanisms of atmosphere-ocean interaction under stormy weather conditions, Probl Arct Antarct, 43, 73-83, 1974.

Bortkovskii, R.: On the mechanism of interaction between the ocean and the atmosphere during a storm, Fluid Mech Sov Res, 2, 87-94, 1973.

Burk, S. D.: The generation, turbulent transfer and deposition of the sea-salt aerosol, Journal of Atmospheric Sciences, 41, 3040-3051, 1984.

Ceppi, P., Hwang, Y. T., Frierson, D. M., and Hartmann, D. L.: Southern Hemisphere jet latitude biases in CMIP5 models linked to shortwave cloud forcing, Geophysical Research Letters, 39, 2012.

Djurdjevic, V., and Rajkovic, B.: Verification of a coupled atmosphere-ocean model using satellite observations over the Adriatic Sea, Annales Geophysicae, 2008, 1935-1954,

Edson, J. B., and Andreas, E. L.: Modeling the role of sea spray on air-sea heat and moisture exchange, Final Rep, 6, 18, 1997.

Emanuel, K. A.: Sensitivity of tropical cyclones to surface exchange coefficients and a revised steadystate model incorporating eye dynamics, Journal of Atmospheric Sciences, 52, 3969-3976, 1995.

Fairall, C., Davidson, K., and Schacher, G.: An analysis of the surface production of sea - salt aerosols, Tellus B, 35, 31-39, 1983.

Fairall, C., and Larsen, S. E.: Dry deposition, surface production and dynamics of aerosols in the marine boundary layer, Atmospheric Environment (1967), 18, 69-77, 1984.

Fairall, C., Kepert, J., and Holland, G.: The effect of sea spray on surface energy transports over the ocean, Global Atmos. Ocean Syst, 2, 121-142, 1994.

Fairall, C., Bradley, E. F., Rogers, D. P., Edson, J. B., and Young, G. S.: Bulk parameterization of air - sea fluxes for tropical ocean - global atmosphere coupled - ocean atmosphere response experiment, Journal of Geophysical Research: Oceans, 101, 3747-3764, 1996.

Fox-Kemper, B., Johnson, L., and Qiao, F.: Ocean near-surface layers, in: Ocean Mixing, Elsevier, 65-94, 2022.

Garg, N., Ng, E. Y. K., and Narasimalu, S.: The effects of sea spray and atmosphere–wave coupling on air–sea exchange during a tropical cyclone, Atmospheric Chemistry and Physics, 18, 6001-6021, 2018.

Gauss, C. F.: Methodvs nova integralivm valores per approximationem inveniendi, apvd Henricvm Dieterich, 1815.

Griffies, S. M., Harrison, M. J., Pacanowski, R. C., and Rosati, A.: A technical guide to MOM4, GFDL Ocean Group Tech. Rep, 5, 342, 2004.

WAVEWATCH III Development Group: User manual and system documentation of WAVEWATCH III version 5.16, NOAA/NWS/NCEP/MMAB Technical Note 329, 326, 2016.

Hersbach, H., Bell, B., Berrisford, P., Hirahara, S., Horányi, A., Muñoz - Sabater, J., Nicolas, J., Peubey, C., Radu, R., and Schepers, D.: The ERA5 global reanalysis, Quarterly Journal of the Royal Meteorological Society, 146, 1999-2049, 2020.

Jacobi, C. G. J.: Ueber Gauss neue Methode, die Werthe der Integrale näherungsweise zu finden, 1826.

Kalnay, E., Kanamitsu, M., Kistler, R., Collins, W. D., Deaven, D. G., Gandin, L. S., Iredell, M. D., Saha, S., White, G. H., and Woollen, J.: The NCEP/NCAR 40-Year Reanalysis Project, Bulletin of the American Meteorological Society, 77, 437-471, http://dx.doi.org/10.1175/1520-0477(1996)077%3C0437:TNYRP%3E2.0.CO;2, 1996.

Koga, M.: Direct production of droplets from breaking wind‐waves—its observation by a multi‐colored overlapping exposure photographing technique, Tellus, 33, 552-563, 1981.

Lhuissier, H., and Villermaux, E.: Bursting bubble aerosols, Journal of Fluid Mechanics, 696, 5-44, 2012.

Li, J., Waliser, D., Stephens, G., Lee, S., L'Ecuyer, T., Kato, S., Loeb, N., and Ma, H. Y.: Characterizing and understanding radiation budget biases in CMIP3/CMIP5 GCMs, contemporary GCM, and reanalysis, Journal of Geophysical Research: Atmospheres, 118, 8166-8184, 2013.

Li, J. N., and Barker, H. W.: Computation of domain‐average radiative flux profiles using Gaussian quadrature, Quarterly Journal of the Royal Meteorological Society, 144, 720-734, 2018.

Lindemann, D., Avila-Diaz, A., Pezzi, L., Rodrigues, J., Freitas, R. A., Coelho, L., Alonso, M., and Cerón, W. L.: The Surface Wind Influence on the Heat Fluxes Variability on the South Atlantic, 2021.

Ling, S., and Kao, T.: Parameterization of the moisture and heat transfer process over the ocean under whitecap sea states, Journal of Physical Oceanography, 6, 306-315, 1976.

Liu, B., Guan, C., Xie, L. a., and Zhao, D.: An investigation of the effects of wave state and sea spray on an idealized typhoon using an air-sea coupled modeling system, Advances in Atmospheric Sciences, 29, 391-406, 2012.

Liu, L., Zhang, C., Li, R., and Wang, B.: C-Coupler2: a flexible and user-friendly community coupler for model coupling and nesting, Geoscientific Model Development Discussions, 11, 1-63, http://dx.doi.org/10.5194/gmd-11-3557-2018, 2018.

Liu, L., Wang, G., Zhang, Z., and Wang, H.: Effects of drag coefficients on surface heat flux during Typhoon Kalmaegi (2014), Advances in Atmospheric Sciences, 39, 1501-1518, 2022.

McClarren, R.: Gauss Quadrature and Multi-dimensional Integrals, Computational Nuclear Engineering and Radiological Science Using Python; Academic Press: Cambridge, MA, USA, 287-299, 2018.

Melville, W. K.: The role of surface-wave breaking in air-sea interaction, 1996.

Monahan, E., Davidson, K., and Spiel, D.: Whitecap aerosol productivity deduced from simulation tank measurements, Journal of Geophysical Research: Oceans, 87, 8898-8904, 1982.

Monahan, E., and Van Patten, M. A.: The climate and health implications of bubble-mediated sea-air exchange, 1988.

Myslenkov, S., Zelenko, A., Resnyanskii, Y., Arkhipkin, V., and Silvestrova, K.: Quality of the Wind

Wave Forecast in the Black Sea Including Storm Wave Analysis, Sustainability, 13, 13099, 2021.

Pruppacher, H. R., and Klett, J. D.: Microstructure of atmospheric clouds and precipitation, in: Microphysics of Clouds and Precipitation, Springer, 9-55, 1978.

Resch, F., and Afeti, G.: Film drop distributions from bubbles bursting in seawater, Journal of Geophysical Research: Oceans, 96, 10681-10688, 1991.

Reynolds, R. W., Smith, T. M., Liu, C., Chelton, D. B., Casey, K. S., and Schlax, M. G.: Daily High-Resolution-Blended Analyses for Sea Surface Temperature, Journal of Climate, 20, 5473-5496, http://dx.doi.org/10.1175/2007JCLI1824.1, 2007.

Saha, S., Moorthi, S., Wu, X., Wang, J., Nadiga, S., Tripp, P., Behringer, D., Hou, Y., Chuang, H., and Iredell, M. D.: The NCEP Climate Forecast System Version 2, Journal of Climate, 27, 2185-2208, http://dx.doi.org/10.1175/JCLI-D-12-00823.1, 2014.

Seethala, C., Zuidema, P., Edson, J., Brunke, M., Chen, G., Li, X. Y., Painemal, D., Robinson, C., Shingler, T., and Shook, M.: On assessing ERA5 and MERRA2 representations of cold‐air outbreaks across the Gulf Stream, Geophysical research letters, 48, e2021GL094364, 2021.

Shi, R., Xu, F., Liu, L., Fan, Z., Yu, H., Li, H., Li, X., and Zhang, Y.: The effects of ocean surface waves on global intraseasonal prediction: case studies with a coupled CFSv2. 0–WW3 system, Geoscientific Model Development, 15, 2345-2363, 2022.

Smith, R. K.: On the theory of CISK, Quarterly Journal of the Royal Meteorological Society, 123, 407-418, 1997.

Smith, R. K., Montgomery, M. T., and Thomsen, G. L.: Sensitivity of tropical‐cyclone models to the surface drag coefficient in different boundary‐layer schemes, Quarterly Journal of the Royal Meteorological Society, 140, 792-804, 2014.

Song, Y., Qiao, F., Liu, J., Shu, Q., Bao, Y., Wei, M., and Song, Z.: Effects of sea spray on large-scale climatic features over the Southern Ocean, Journal of Climate, 1-51, 2022.

Spiel, D. E.: More on the births of jet drops from bubbles bursting on seawater surfaces, Journal of Geophysical Research: Oceans, 102, 5815-5821, 1997.

Thorpe, S.: Bubble clouds and the dynamics of the upper ocean, Quarterly Journal of the Royal Meteorological Society, 118, 1-22, 1992.

Troitskaya, Y., Kandaurov, A., Ermakova, O., Kozlov, D., Sergeev, D., and Zilitinkevich, S.: The "bag breakup" spume droplet generation mechanism at high winds. Part I: Spray generation function, Journal of physical oceanography, 48, 2167-2188, 2018.

Van Eijk, A., Kusmierczyk‐Michulec, J., Francius, M., Tedeschi, G., Piazzola, J., Merritt, D., and Fontana, J.: Sea‐spray aerosol particles generated in the surf zone, Journal of Geophysical Research: Atmospheres, 116, 2011.

Veron, F.: Ocean spray, Annu. Rev. Fluid Mech, 47, 507-538, 2015.

Wang, C., Zhang, L., Lee, S.-K., Wu, L., and Mechoso, C. R.: A global perspective on CMIP5 climate model biases, Nature Climate Change, 4, 201-205, 2014.

Wu, J.: Evaporation due to spray, Journal of Geophysical Research, 79, 4107-4109, 1974.

Wu, L., Cheng, X., Zeng, Q., Jin, J., Huang, J., and Feng, Y.: On the upward flux of sea‐spray spume droplets in high‐wind conditions, Journal of Geophysical Research: Atmospheres, 122, 5976-5987, 2017.

Xu, X., Voermans, J., Liu, Q., Moon, I.-J., Guan, C., and Babanin, A.: Impacts of the Wave-Dependent Sea Spray Parameterizations on Air–Sea–Wave Coupled Modeling under an Idealized Tropical Cyclone, Journal of Marine Science and Engineering, 9, 1390, 2021a.

Xu, X., Voermans, J., Ma, H., Guan, C., and Babanin, A. V.: A Wind–Wave-Dependent Sea Spray Volume Flux Model Based on Field Experiments, Journal of Marine Science and Engineering, 9, 1168, 2021b.

Yu, L., Jin, X., and Weller, R. A.: 2008: Multidecade global flux datasets from the Objectively Analyzed Air-Sea Fluxes (OAFlux) Project: Latent and sensible heat fluxes, ocean evaporation, and related surface meteorological variables. Woods Hole Oceanographic Institution OAFlux Project Tec, Rep, 2008,

Zhao, B., Qiao, F., Cavaleri, L., Wang, G., Bertotti, L., and Liu, L.: Sensitivity of typhoon modeling to surface waves and rainfall, Journal of Geophysical Research: Oceans, 122, 1702-1723, 2017.

Table 1. The runtime of CFSv2.0-WW3 global experiments for 7-day forecast with different parameterizations.

7-day Forecast	Runtime (h)
SPRAY-A92	126.94
SPRAY-A15	7.60
SPRAY-GQ	7.67

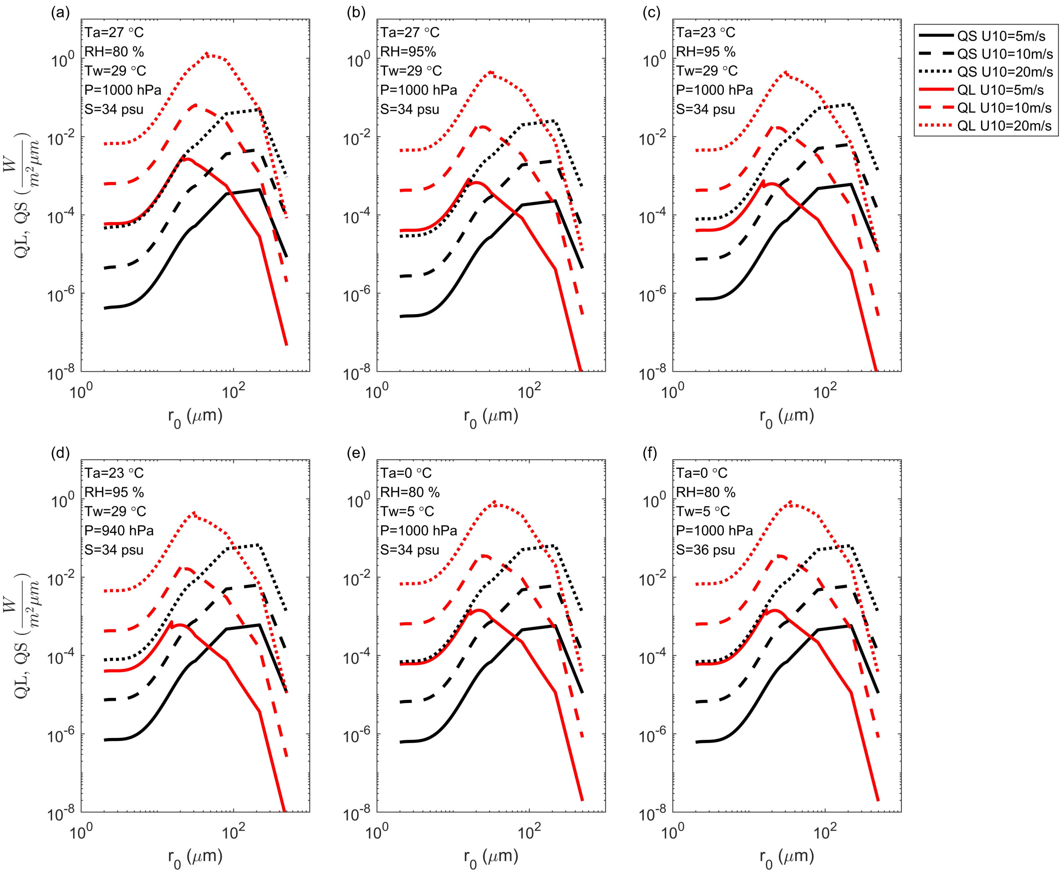

Figure 1. The radius-specific sea spray-mediated sensible (Q_S; black) and latent (Q_L; red) heat fluxes as functions of initial radius r_0: U_{10}, Ta, RH, Tw, P and S are 10-m wind speed, 2-m air temperature, 2-m relative humidity, sea surface temperature, surface air pressure and surface salinity, respectively.

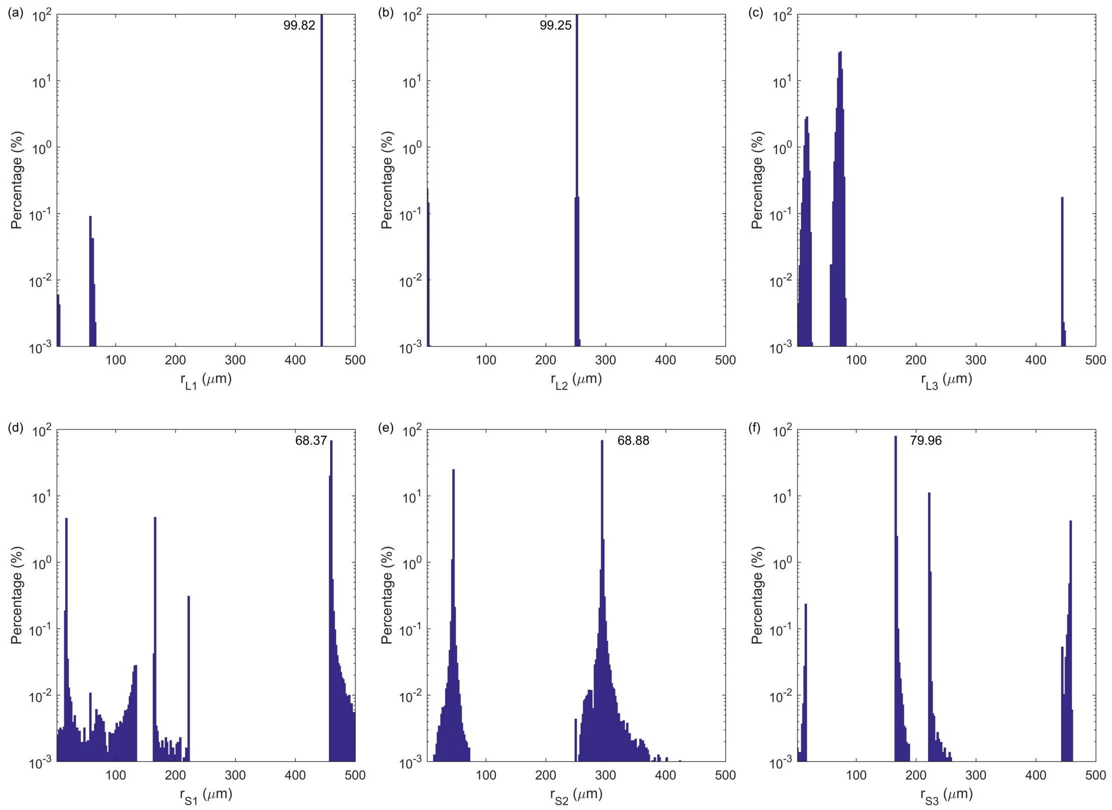

Figure 2. The distribution of occurrence frequency in percentage for GQ radius nodes: (a) the first node of latent heat flux; (b) the second node of latent heat flux; (c) the third node of latent heat flux; (d) the first node of sensible heat flux; (e) the second node of sensible heat flux; (f) the third node of sensible heat flux. The peak frequencies are marked.

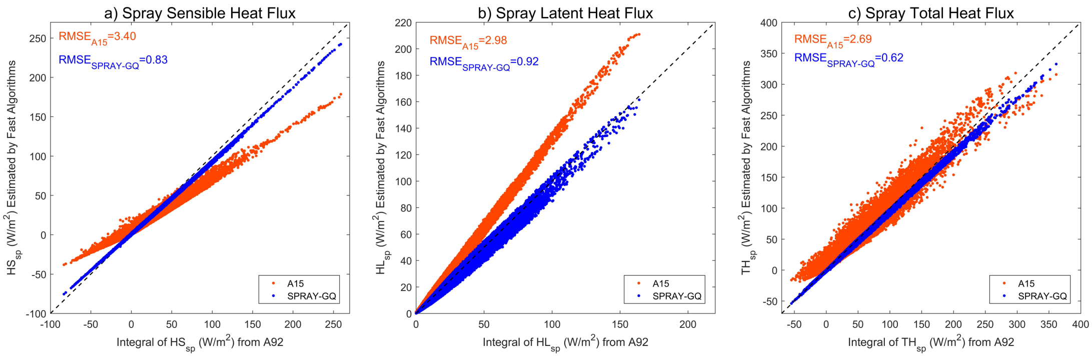

Figure 3. Scatter plots of $H_{S,SP}$ (a), $H_{L,SP}$ (b) and total heat flux $TH_{SP} = H_{S,SP}$+$H_{L,SP}$ (c) estimated by fast algorithms (y-axis) vs those estimated by spectral integral in microphysical parameterization (x-axis): The dotted black line is y=x. The corresponding RMSEs are marked in the upper left corner.

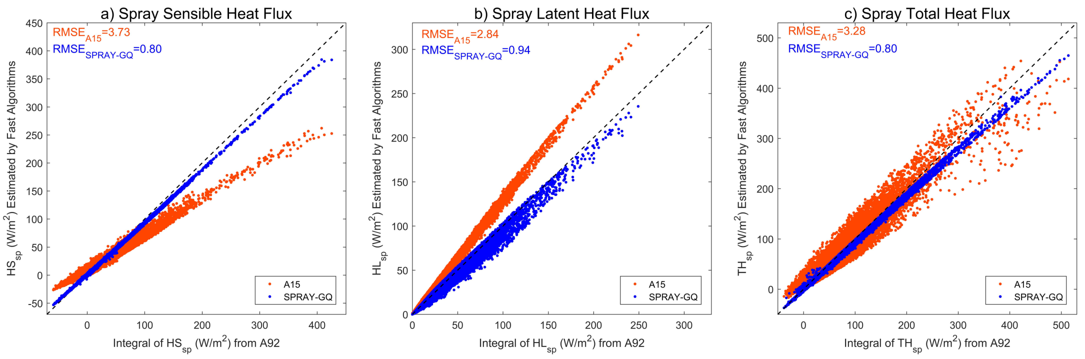

Figure 4. The same as Figure 3, but WSP10, 2-m air temperature and 2-m specific humidity of OAFlux are used.

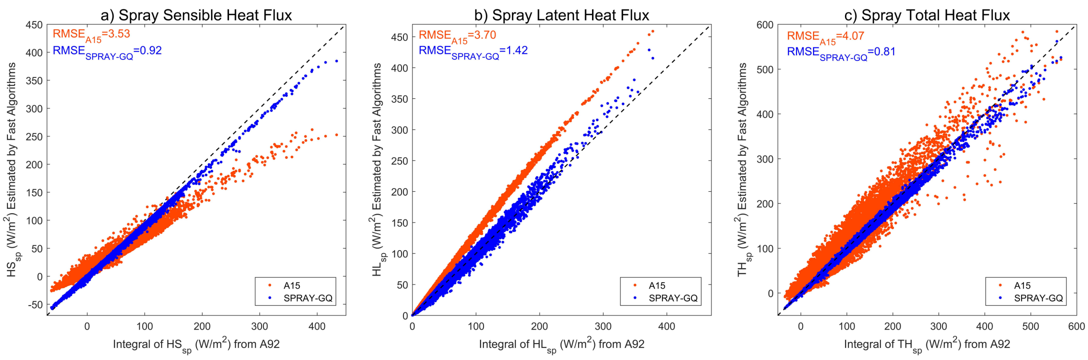

Figure 5. The same as Figure 4, but SWH is derived by WSP10 instead of ERA5 SWH.

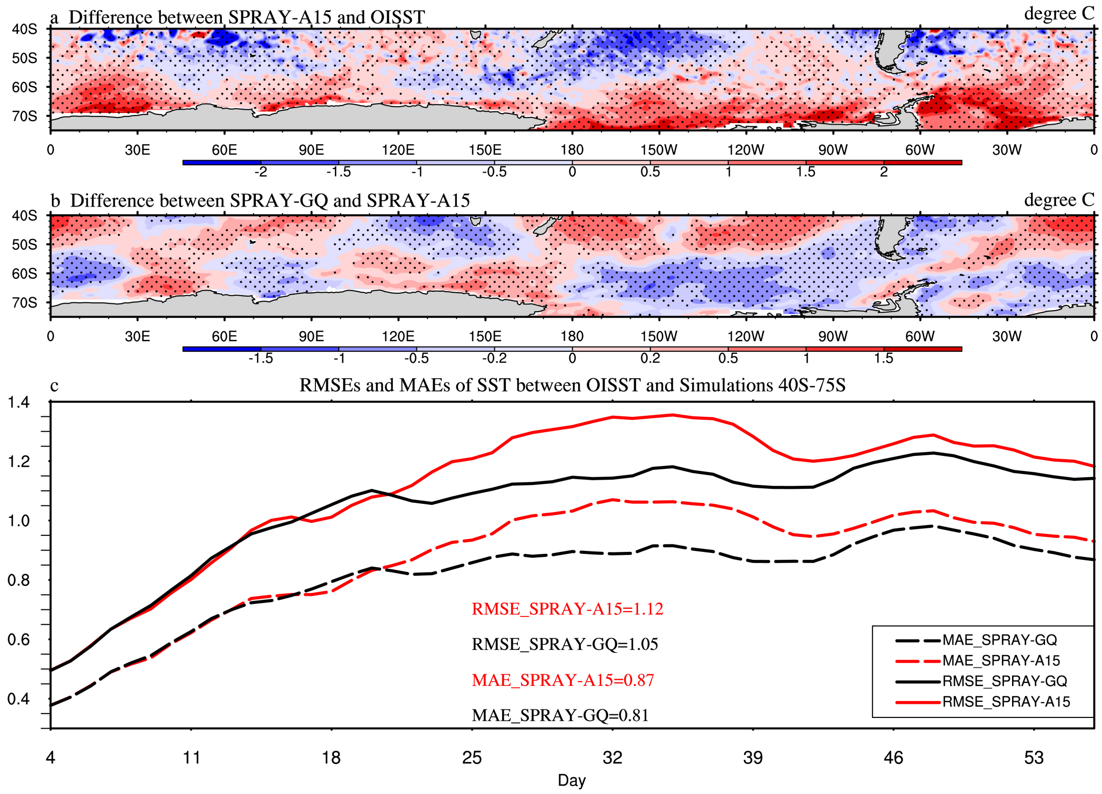

Figure 6. The 53-day average SST (°C) differences between SPRAY-A15 and OISST (a; SPRAY-A15 minus OISST), the differences between SPRAY-GQ and SPRAY-A15 (b; SPRAY-GQ minus SPRAY-A15), and the time series of domain-averaged RMSE and MAE (c; 0-360°E, 40-75°S) in Jan-Feb, 2017. The first 3-day simulation is discarded. The dotted areas are statistically significant at 95% confidence level.

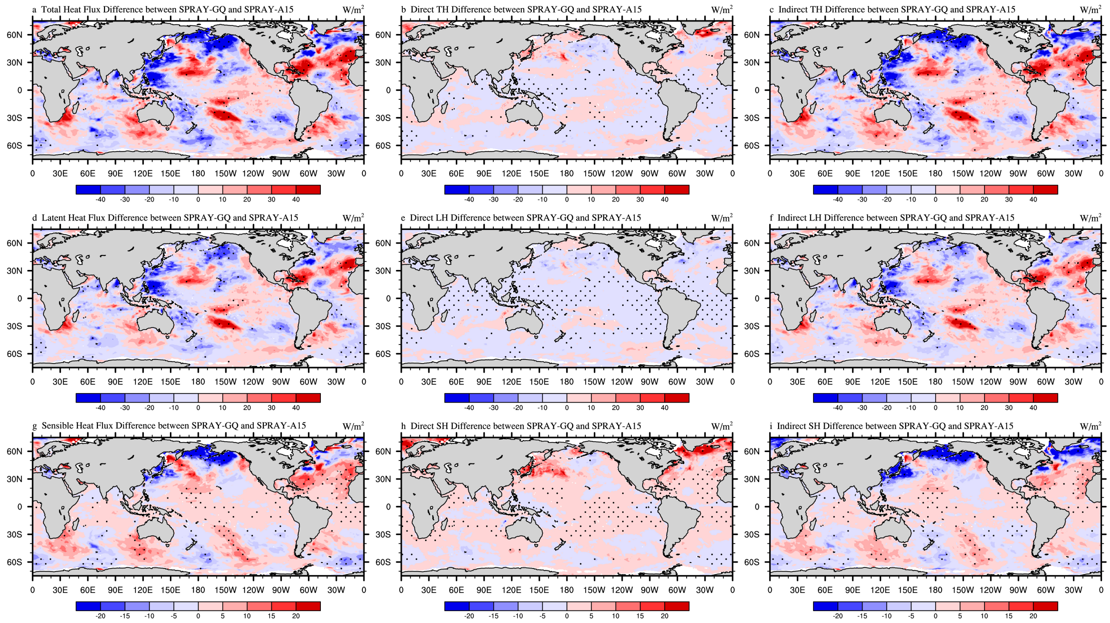

Figure 7. The 53-day average differences of total heat flux (a-c), latent heat flux (d-f), and sensible heat flux (g-i) between SPRAY-GQ and SPRAY-A15 (SPRAY-GQ minus SPRAY-A15) in Jan-Feb, 2017. The direct differences indicate sea spray-mediated heat flux differences (b, e, h), and the indirect differences indicate interfacial (bulk) heat flux differences resulted by sea spray (c, f, i). The dotted areas are statistically significant at 95% confidence level. A positive value of flux indicates an upward direction.

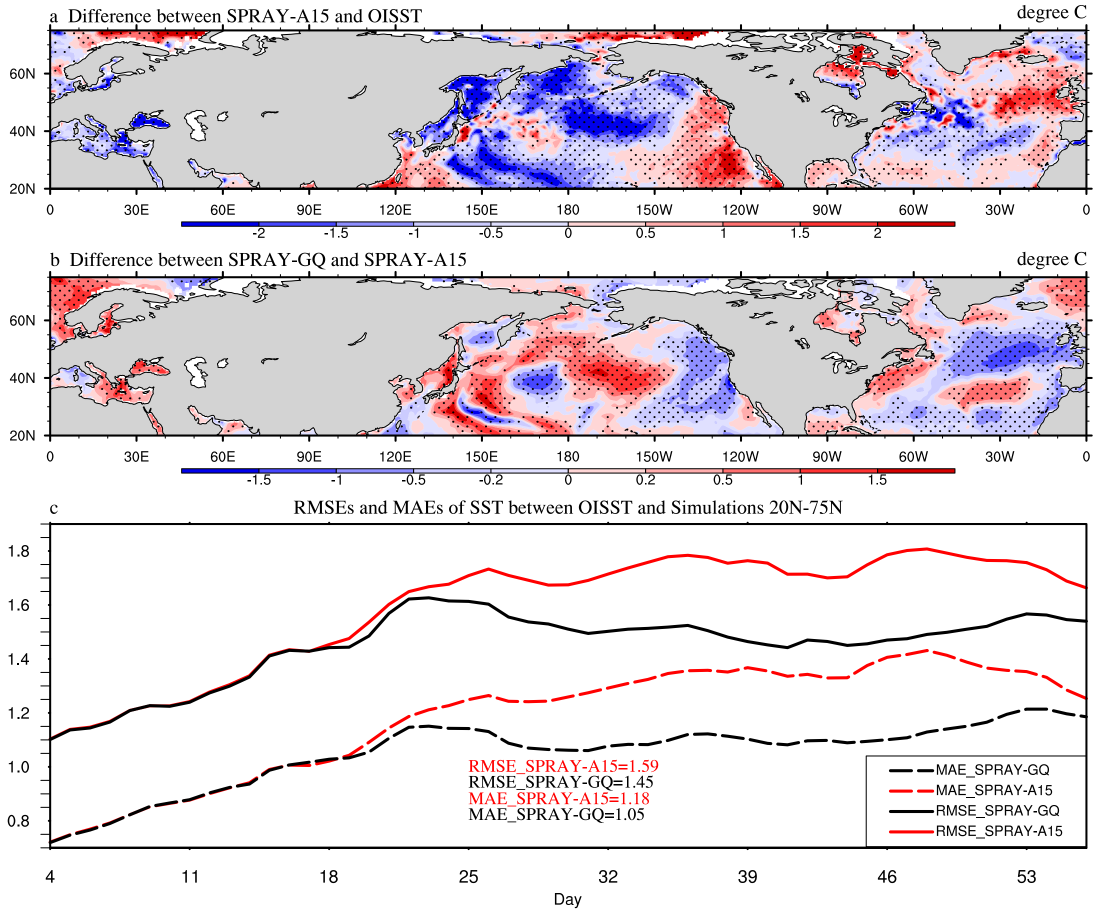

Figure 8. The same as Figure 6, but for Aug-Sep, 2018 in 0-360°E, 20-75°N.

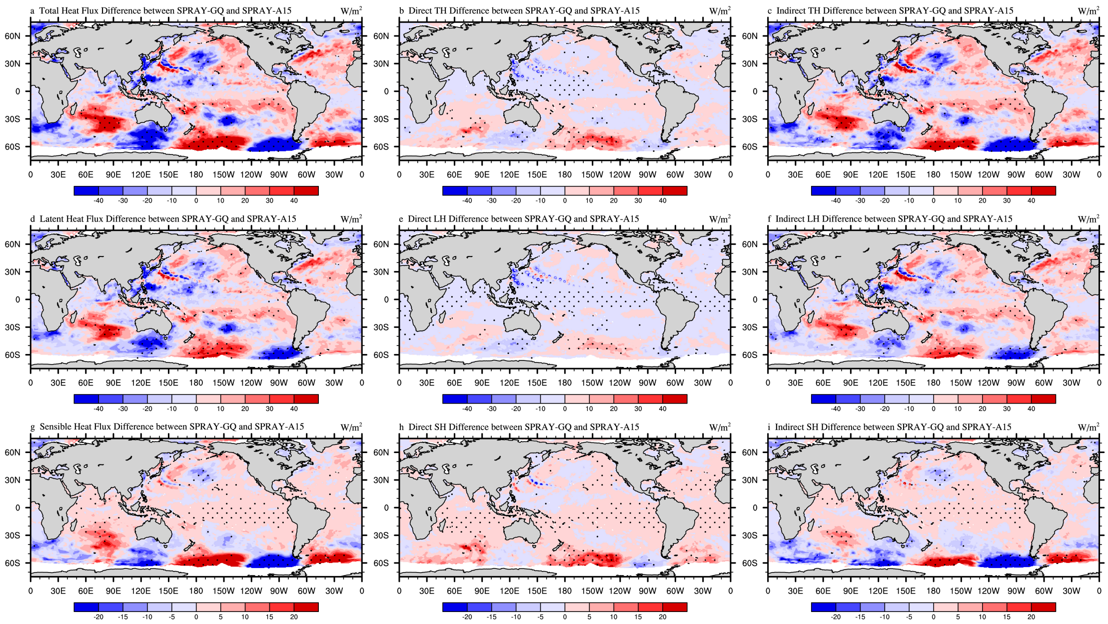

Figure 9. The same as Figure 7, but for Aug-Sep, 2018.

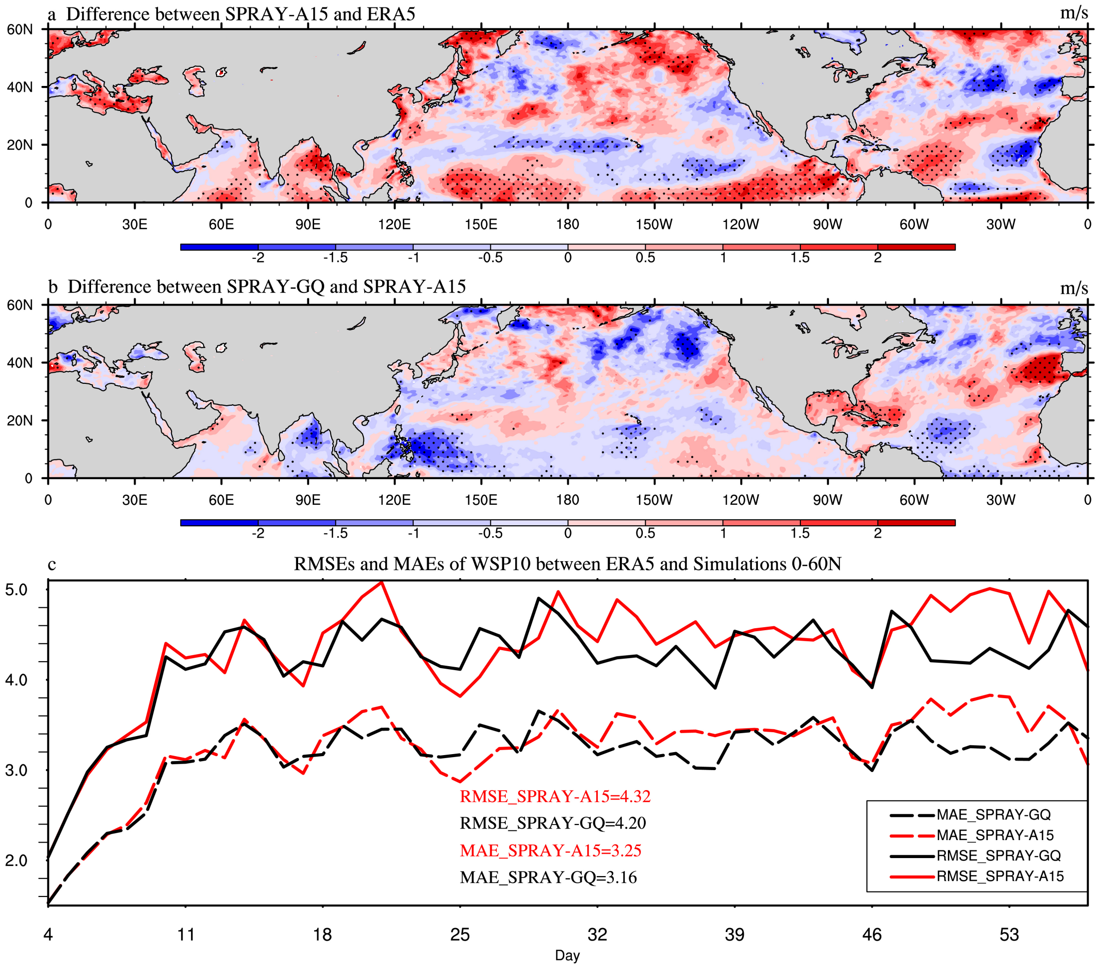

Figure 10. The 53-day average WSP10 (m/s) differences between SPRAY-A15 and ERA5 (a; SPRAY-A15 minus ERA5), the differences between SPRAY-GQ and SPRAY-A15 (b; SPRAY-GQ minus SPRAY-A15), and the time series of domain-averaged RMSE and MAE (c; 0-360°E, 0-60°N) in Jan-Feb, 2017. The first 3-day simulation is discarded. The dotted areas are statistically significant at 95% confidence level.

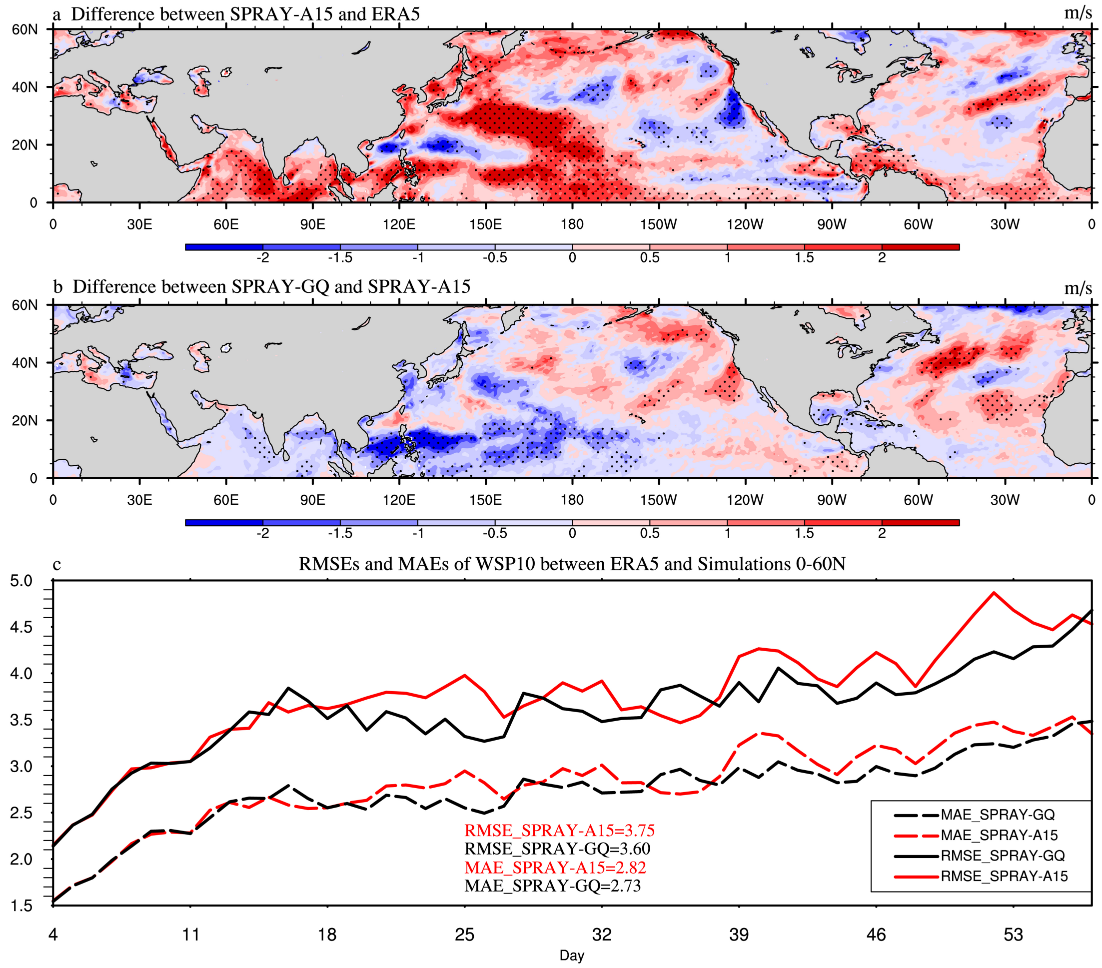

Figure 11. The same as Figure 10, but for Aug-Sep, 2018.

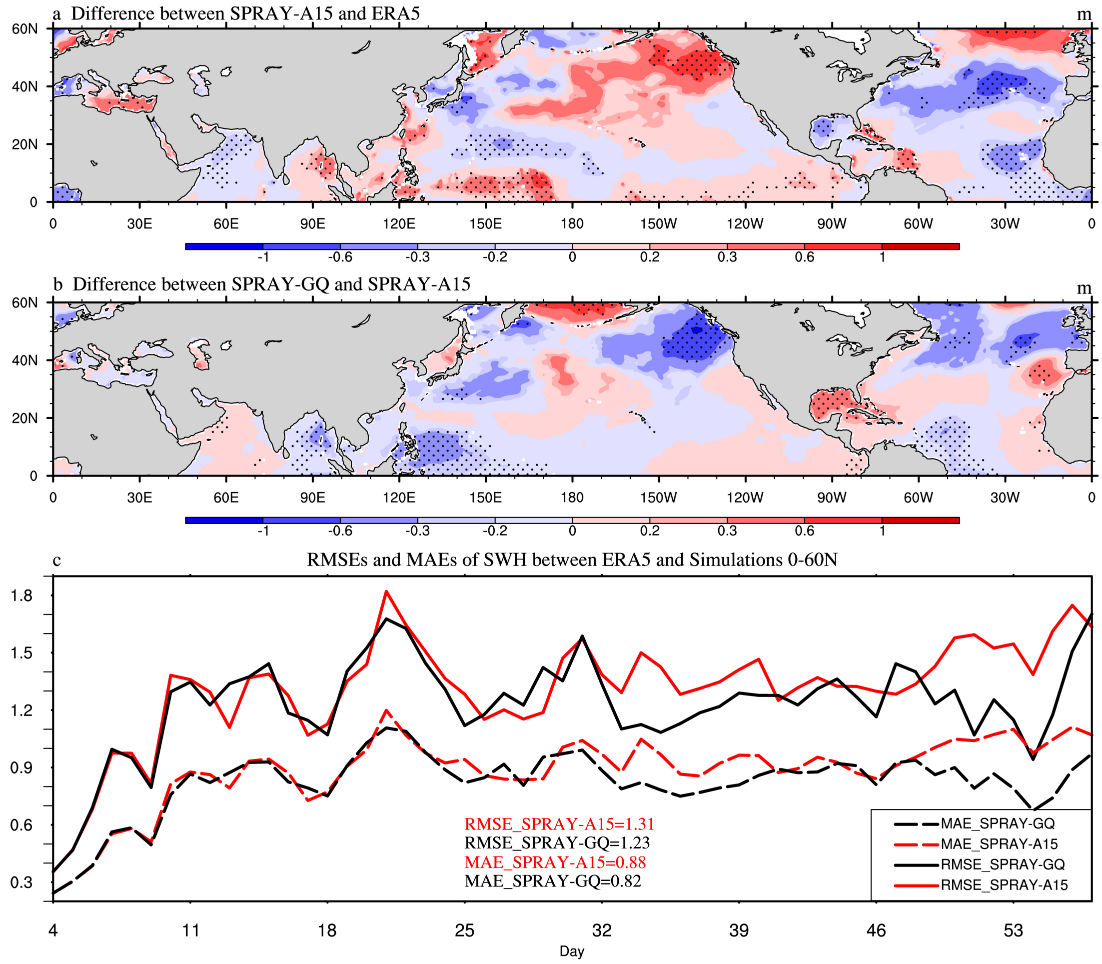

Figure 12. The 53-day average SWH (m) differences between SPRAY-A15 and ERA5 (a; SPRAY-A15 minus ERA5), the differences between SPRAY-GQ and SPRAY-A15 (b; SPRAY-GQ minus SPRAY-A15), and the time series of domain-averaged RMSE and MAE (c; 0-360°E, 0-60°N) in Jan-Feb, 2017. The first 3-day simulation is discarded. The dotted areas are statistically significant at 95% confidence level.

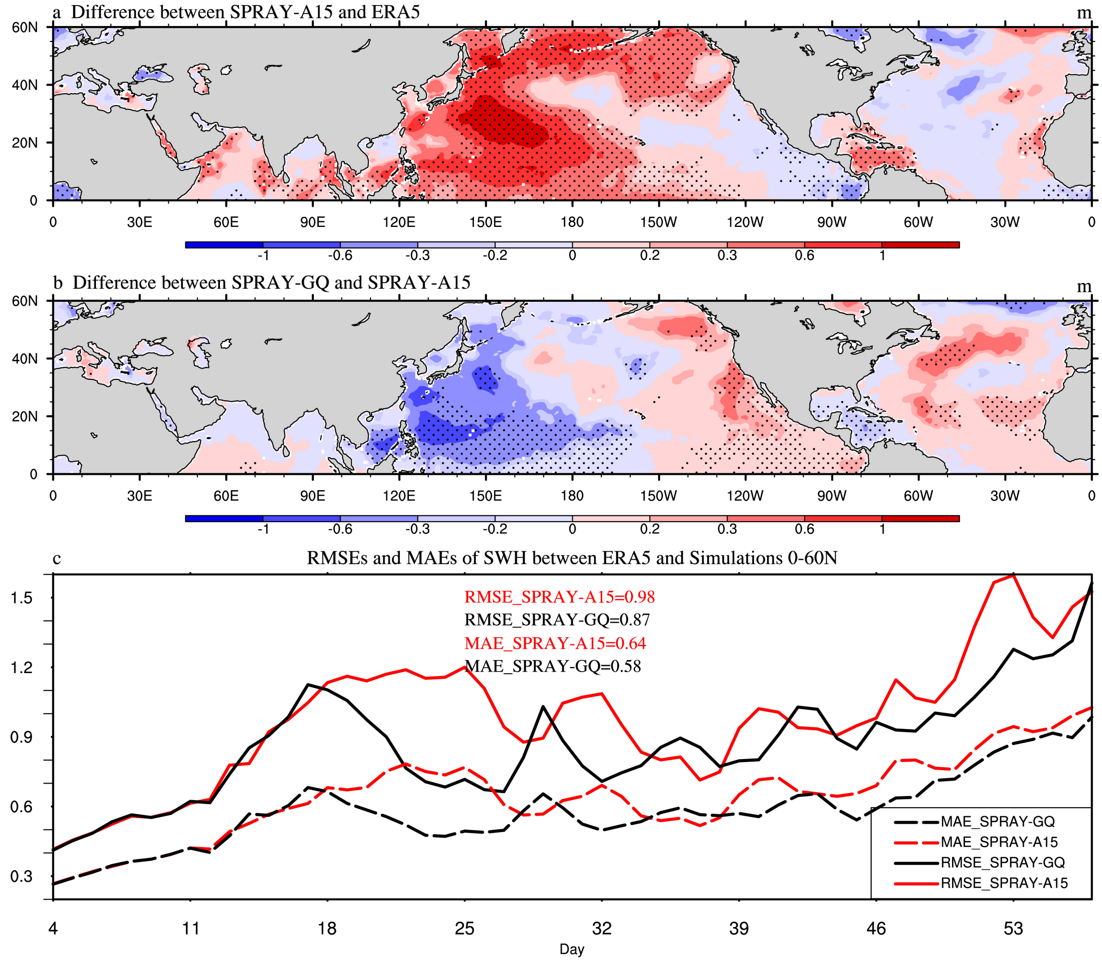

Figure 13. The same as Figure 12, but for Aug-Sep, 2018.